Multiconfigurational g Tensor Calculations as a Probe for the Covalency of the Copper−Ligand Bonds in Copper(II) Complexes: $[CuCl_4]^{2-}$, $[Cu(NH_3)_4]^{2+}$, and Plastocyanin

Steven Vancoillie and Kristine Pierloot*

Department of Chemistry, University of Leuven Celestijnenlaan, 200F B-3001 Heverlee-Leuven, Belgium

Received: November 30, 2007; In Final Form: February 14, 2008

Calculations of the **g** tensor of three copper(II) complexes $[Cu(NH_3)_4]^{2+}$, $[CuCl_4]^{2-}$, and plastocyanin are presented. Two different sum-over-states-based approaches are considered, making use of the multistate CASPT2 method for excitation energies and PMCAS (perturbation modified CAS) wave functions for the computation of the angular momentum and spin−orbit coupling matrix elements. Test calculations on $[Cu(NH_3)_4]^{2+}$ and $[CuCl_4]^{2-}$ point to the need of including in the MS-CASPT2 treatment the specific charge-transfer state with an electron excited out of the bonding counterpart of the ground-state SOMO. The computed *g* shifts for these two molecules present a considerable improvement with respect to the results obtained from our previous **g** tensor calculations based instead on CASSCF/CASPT2. This is shown to be related to an improved description of the covalency of the Cu−L bonds. For the calculations on plastocyanin, different models are used, taken from a recent (QM/MM) DFT study by Sinnecker and Neese. The effect of the surrounding protein is taken into account by surrounding the central cluster either with a dielectric continuum ($\epsilon = 4$) or with a set of point charges. The second approach is found to be indispensable for an accurate description of environmental effects. With this approach, the calculated *g* values compare to within 30 ppt with the experimental data of plastocyanin.

1. Introduction

An important means of studying the electronic structure of transition metals in proteins and other surroundings is EPR (electron paramagnetic resonance) spectroscopy. This technique requires a complex (with unpaired electrons) to be put in an external magnetic field. The resulting splitting of the energy levels is then probed with microwave radiation. EPR spectra are analyzed using the concept of a spin Hamiltonian. This model Hamiltonian describes the splitting using only spin degrees of freedom and a set of parameters. One of these parameters is the **g** tensor, which parametrizes the Zeeman effect arising from the interaction of the total electronic magnetic dipole moment with an external magnetic field. The part of the spin Hamiltonian that describes this interaction is

$$\mathscr{H}_S = \beta \mathbf{B}\cdot\mathbf{g}\cdot\tilde{\mathbf{S}}$$

with **B** the external magnetic field, **g** the molecular **g** tensor, and $\tilde{\mathbf{S}}$ an effective spin operator. By matching the energy splitting produced by this model Hamiltonian with the experimental data, one obtains the *g* values. On the other hand, to calculate the *g* values, one needs to compare the energy splitting produced by the model Hamiltonian with the energy splitting obtained through the physical Hamiltonian. In a recent article,[1] we have implemented two approaches for calculating the **g** tensor in the MOLCAS quantum chemistry software. Both approaches are based on the CASSCF/CASPT2 method (complete active space self-consistent field with second-order perturbation theory), which has, by now, proven itself to be the most efficient choice for ab initio calculations on large transition-metal complexes.[2−4] The **g** tensor is obtained using the RASSI-SO (restricted active space state interaction spin−orbit coupling) scheme with the AMFI (atomic mean field integrals) approximation for spin−orbit coupling. The total angular momentum and spin−orbit coupling matrix elements are obtained from CASSCF wave functions. Excitation energies are obtained from CASPT2 calculations.

However, for calculating the **g** tensor for copper(II) complexes, some difficulties where encountered. Specifically, we found that the CASSCF method was unable to correctly describe the covalency of the Cu−L (copper−ligand) bonds. Both in $[Cu(NH_3)_4]^{2+}$ and in $[CuCl_4]^{2-}$, the Cu−L interaction was found to be too ionic. As such, the calculated orbital angular momentum and spin−orbit coupling matrix elements were too large. This resulted in Δg values that were a factor of 1.5−2.0 higher than the experimental Δg values for $[Cu(NH_3)_4]^{2+}$ and $[CuCl_4]^{2-}$, respectively.

In this work, we investigate what happens if the original CASSCF reference wave functions of the ground state and specific excited states are allowed to interact under the influence of dynamical correlation, using the multistate CASPT2 (MS-CASPT2) method.[5] This method was devised to treat cases where the CASSCF wave function is not a good reference function for the perturbation treatment due to coupling between different electronic states through dynamical correlation. Typical cases are avoided crossings on potential energy surfaces and valence−Rydberg mixing in the electronic spectra of organic molecules. In the present study, the problem is related to the presence of a strong interaction between the ground state (GS) and excited charge-transfer (CT) state(s), corresponding to an excitation of an electron from bonding ligand−Cu 3d combination(s) into the GS SOMO, that is, the orbital that is singly

* To whom correspondence should be addressed. Fax: +32 16 32 79 92. E-mail: kristin.pierloot@chem.kuleuven.be.

10.1021/jp711345n CCC: $40.75 © 2008 American Chemical Society
Published on Web 04/03/2008

occupied in the ground state of the Cu(II) complex. The method will first be applied to $[Cu(NH_3)_4]^{2+}$ and $[CuCl_4]^{2-}$. Second, we apply our findings to the calculation of the **g** tensor in plastocyanin.

Plastocyanin belongs to the class of blue copper proteins, named after their copper-containing active site and blue color. The latter is the result of an intense absorption in the 600 nm region of the electromagnetic spectrum (16 000 cm^{-1}). A typical feature of this type of proteins is a high reduction potential, related to their involvement in electron-transfer processes. Plastocyanin in particular is a rather small protein which acts as an electron transportation service.

The electronic structure of plastocyanin is characterized by a highly covalent $Cu-S_{Cys}$ π bond. The absorption band at 16 000 cm^{-1} originates from a charge-transfer excitation from the bonding to the antibonding Cu $3d-S_{Cys}$ $3p_\pi$ combination, gaining its intensity from the large overlap between the two orbitals involved. This has been shown in several theoretical studies of the electronic spectrum of plastocyanin.[6−10] At higher energy (22 000 cm^{-1}), a second charge-transfer band appears in the spectrum, corresponding to an excitation out of the bonding Cu $3d-S_{Cys}$ $3p_\sigma$ combination. The second band is relatively weak in plastocyanin (and other axial blue Cu proteins, e.g., azurin) but becomes much more prominent in other (rhombic) proteins like pseudoazurin and nitrite reductase, where, due to a flattening of the structure from trigonal to square-planar, the SOMO gains more S_{Cys} σ character at the expense of S_{Cys} π character.[11]

Whereas electronic absorption spectra of several blue copper proteins have been extensively studied by means of different quantum chemical methods,[6−15] accurate theoretical studies of the EPR spectra are more scarce. Several semiempirical (ligand field) and DFT (density functional theory) studies are available, providing a comprehensive but often qualitative explanation of the EPR spectra.[7,12,16−22] To our knowledge, only one ab initio (multireference determinantal configuration interaction) study has previously been reported for the **g** tensor of azurin.[23] More recently, Sinnecker and Neese have reported a QM/MM study on plastocyanin using DFT (B3LYP).[24] The main purpose of this study was to determine how the EPR and optical spectra are influenced by the surrounding protein. While the results were qualitatively correct, remaining errors were substantial and could be traced back to the "stiffness" of the linear response of the available functionals with respect to the external perturbations. The most recent theoretical work concerns a DFT study of three blue copper proteins, azurin, plastocyanin, and stellacyanin,[25] focusing in particular on the dependence of the EPR parameters on the admixture of exact exchange in hybrid density functionals.

Herein, we present an ab initio treatment of the EPR **g** tensor (including the optical spectrum) of plastocyanin using the same model complexes introduced by Sinnecker and Neese.

2. Computational Details

All CASSCF[26]/CASPT2[27,28] and **g** tensor calculations were performed with MOLCAS 6.4.[29] All-electron basis sets were used throughout. Scalar relativistic effects were included using a DKH Hamiltonian.[30−32] For each molecule, the ground-state and excited-state wave functions were computed at the CASSCF level. The excitation energies were computed at the CASPT2 level. In all CASPT2 calculations, the core electrons were kept frozen, except for the Cu 3s,3p orbitals. An imaginary level shift[33,34] of 0.1 was used to avoid intruder states. The **g** tensor calculations were performed with the RASSI module, which treats spin−orbit coupling using the AMFI[35−37] approximation.

In our previous study,[1] two different approaches for calculating the **g** tensor were introduced. Approach I treats spin−orbit coupling and the Zeeman effect through second-order perturbation theory

$$g_{pq} = \delta_{pq} g_e - f_a \sum_b \Delta_b^{-1} [\langle a|\sum_i \hat{l}_p(i)|b\rangle\langle bS_a|\sum_i \hat{h}_q(i)|aS_a\rangle + \langle aS_a|\sum_i \hat{h}_q(i)|bS_a\rangle\langle b|\sum_i \hat{l}_p(i)|a\rangle] \quad (1)$$

whereas approach II includes the Zeeman effect through first-order degenerate perturbation theory in an isolated Kramers doublet

$$G_{pq} = 2 \sum_{\phi_k,\phi_l} \langle\phi_k|\hat{L}_p + g_e\hat{S}_p|\phi_l\rangle\langle\phi_l|\hat{L}_q + g_e\hat{S}_q|\phi_k\rangle \quad (2)$$

The diagonal g values are then obtained by diagonalizing the **G** tensor and taking the square root of the diagonal G values. For more details regarding both approaches, we refer the reader to ref 1.

The following point groups were used for the CASSCF/CASPT2 calculations: D_{2h} for $[CuCl_4]^{2-}$ (D_{4h}), D_2 for $[Cu(NH_3)_4]^{2+}$ (D_{2d}), and C_1 for the plastocyanin models, with the structural symmetry in parentheses.

For the molecules $[Cu(NH_3)_4]^{2+}$ and $[CuCl_4]^{2-}$, ANO-RCC basis sets were used for all elements and contracted as follows: [7s6p5d3f2g1h] for Cu, [5s4p2d1f] for Cl, [4s3p2d1f] for N, and [3s2p1d] for H. The copper−ligand distances in both molecules were optimized at the CASPT2 level of theory using a pointwise method. For $[Cu(NH_3)_4]^{2+}$, the other coordinates were optimized with PBE0-DFT for each Cu−N distance used for the CASPT2 optimization.

Two complexes were used to model the blue copper site in plastocyanin, PCU-S and PCU-L. The PCU-S model consists of the copper atom and truncated models of the four directly bonded amino acid residues His37, His87, Met92, and Cys84. Cys84 is modeled by CH_3S^-, Met92 by $(CH_3)_2S$, and His37 and 87 by CH_3Im (Im = imidazole). For the PCU-L model, the full amino acid residues His37, His87, Met92, and Cys84 are used, together with the Asn38 residue. The latter is added to account for the hydrogen bond between the Asn38 and Cys84 residues, which was found to be important to describe the correct electronic structure of the active site.[38] For the plastocyanin model PCU-S, two basis sets were used, denoted as A and B. The PCU-L model was only feasible with the smaller basis set A. The contractions used were (A) ANO-RCC [7s6p4d2f] for Cu, ANO-S [5s4p1d] for S, ANO-S [4s3p1d] for N (directly bonded to Cu), ANO-S [3s2p] for C, N (not bonded to Cu), and O, and ANO-S [2s] for H; and (B) ANO-RCC [7s6p5d2f1g] for Cu, ANO-RCC [5s4p1d] for S, ANO-RCC [4s3p1d] for N (directly bonded to Cu), ANO-S [3s2p] for C and N (not bonded to Cu), and ANO-S [2s] for H.

To include the effects of the surrounding protein, Sinnecker and Neese[24] combined molecular dynamics with QM/MM calculations to obtain the geometry of the small PCU-S and large PCU-L models. We adopted the same structures from their work. In the single-point CASPT2 calculations on these structures, the effect of the protein surrounding on the QM/MM structures was either neglected (VAC), included as a polarizable continuum with a dielectric constant of 4 (CONT)[39] (using the PCM model with unified atomic topological model radii implemented in MOLCAS 6.4), or taken into account by including the net charges of all of the atoms from the MM level (PROT).

For all copper(II) complexes considered, the active space consists of nine electrons distributed over the five Cu 3d orbitals together with an extra shell of d orbitals to describe the 3d double-shell effect.[2,40,41] To include important correlation effects associated with the covalent σ bond formed between the ligands and the singly occupied Cu 3d orbital in $[CuCl_4]^{2-}$ and $[Cu(NH_3)_4]^{2+}$, this active space was further extended with the appropriate bonding metal−ligand combination (b_{1g} for $[CuCl_4]^{2-}$ and b_2 for $[Cu(NH_3)_4]^{2+}$), thus arriving at an active space of 11 electrons distributed over 11 orbitals. For the plastocyanin models, both the Cu−S_{Cys} σ and Cu−S_{Cys} π bonding molecular orbitals were included, thus resulting in an active space of 13 electrons in 12 orbitals.

For $[Cu(NH_3)_4]^{2+}$ and $[CuCl_4]^{2-}$, two different sets of CASSCF calculations were performed. In a first set of calculations, individual orbital optimizations were performed for all individual states. In a second set, states belonging to the same symmetry species were calculated with a common average set of optimized orbitals. The latter procedure is bound to give a worse CASSCF description of the ground state. However, it allows us to perform a subsequent MS-CASPT2 calculation. For plastocyanin, only average CASSCF calculations were performed. Since there is no symmetry in this molecule, individual orbital optimizations are impossible because of root flipping.

3. Results and Discussion

3.1. $[Cu(NH_3)_4]^{2+}$ and $[CuCl_4]^{2-}$. The test case copper(II) complexes under study here are $[Cu(NH_3)_4]^{2+}$ and $[CuCl_4]^{2-}$. $[Cu(NH_3)_4]^{2+}$ has D_{2d} symmetry with a $^2B_2$ ground state. The excited states that contribute directly to the g values are the ^2E ($\Delta g_\perp$) and $^2B_1$ ($\Delta g_\parallel$) states. In the case of the D_{4h} $[CuCl_4]^{2-}$ complex, the $^2B_{1g}$ ground state allows direct contributions to the g values from ^2E_g ($\Delta g_\perp$) and $^2B_{2g}$ ($\Delta g_\parallel$) states. The structures and a schematic overview of their electronic structure is given in Figures 1 and 2. These figures include the orbitals with predominant Cu 3d character, as well as the bonding counterpart (b_2 and b_{1g}) of the b_2^* and b_{1g}^* GS SOMOf of the ammine and chloride complex, respectively. The antibonding combinations, b_2^* and b_{1g}^* are mainly localized on the copper center, whereas the bonding combinations are localized on the ligands, thus giving rise to rather ionic Cu−L bonds. The latter is also reflected by the high ground-state (GS) spin population on copper, 0.85 in $[Cu(NH_3)_4]^{2+}$ and 0.84 in $[CuCl_4]^{2-}$.

The results obtained for the excitation energies and Δg values for both molecules are shown in Table 1 ($[Cu(NH_3)_4]^{2+}$) and Table 2 ($[CuCl_4]^{2-}$). The first column of Tables 1 and 2 gives the results of our previous calculation[1] where a different set of orbitals was optimized for the different ligand field (LF) states. The energies were obtained by subsequently performing a single-state CASPT2 calculation for each state. For both complexes, it was found that only LF states contribute to the g values. This can be expected as only CT states originating from bonding orbitals with substantial metal d character give significant contributions to the L and SO matrix elements.[1,16] For both complexes, the only CT state that meets this requirement is the one corresponding to an excitation from the bonding metal−ligand combination with the same symmetry as the SOMO in the ground state. However, for symmetry reasons, there is no direct contribution from this CT state to any of the g values. Approach I gave Δg values of 81 ppt ($\Delta g_\perp$) and 360 ppt ($\Delta g_\parallel$ for $[Cu(NH_3)_4]^{2+}$ and g values of 96 ppt ($\Delta g_\perp$) and 466 ppt ($\Delta g_\parallel$) for $[CuCl_4]^{2-}$. Both $\Delta g_\perp$ and $\Delta g_\parallel$ arise from one single direct contribution of the ^2E and $^2B_1$ ($[Cu(NH_3)_4]^{2+}$) or ^2E_g and $^2B_{2g}$ ($[CuCl_4]^{2-}$) ligand field (LF) states. Taking into account indirect contributions using approach II, slightly smaller values of 70 and 342 ppt for $[Cu(NH_3)_4]^{2+}$ and 78 and 438 ppt for $[CuCl_4]^{2-}$ were obtained for $\Delta g_\perp$ and $\Delta g_\parallel$. As compared to the experimental data, these calculated results are too high by a factor of 1.5 and 2.0 for the ammine and chloride complex, respectively. The excitation energies, however, correspond well with the experimental values. As the g values were too high but the excitation energies were good, it was concluded that the source of the discrepancy must be a too ionic description of the copper−ligand bonds at the CASSCF level, giving rise to too large L and SO matrix elements.

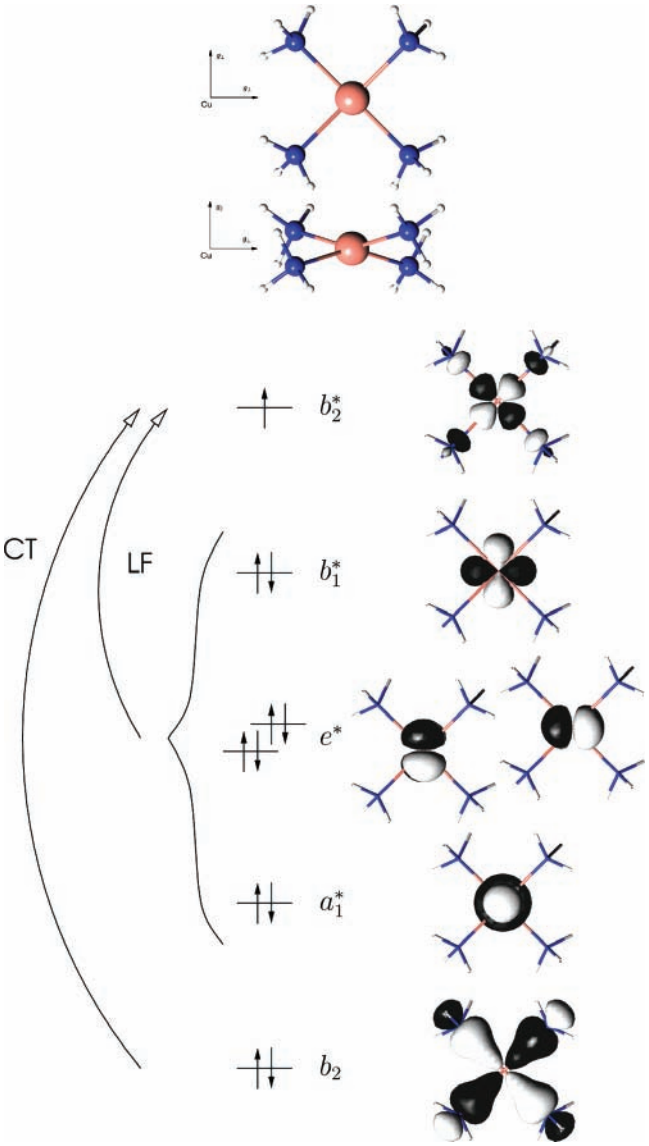

Figure 1. Schematic representation of the geometry and electronic structure of $[Cu(NH_3)_4]^{2+}$.

The results in the second and third column are based on CASSCF reference wave functions, obtained by performing a state-averaged calculation over states that share the same irreducible representation. The states considered are the five LF states as well as the CT state originating from the bonding b_2 or b_{1g} orbital. For the LF excited states, the calculation comes down to a state-specific calculation as each of these states is unique in its irreducible representation. However, the GS CASSCF wave function is now obtained from a calculation including both states in which either the b_2^* (b_{1g}^*) or its bonding counterpart b_2 (b_{1g}) are singly occupied.

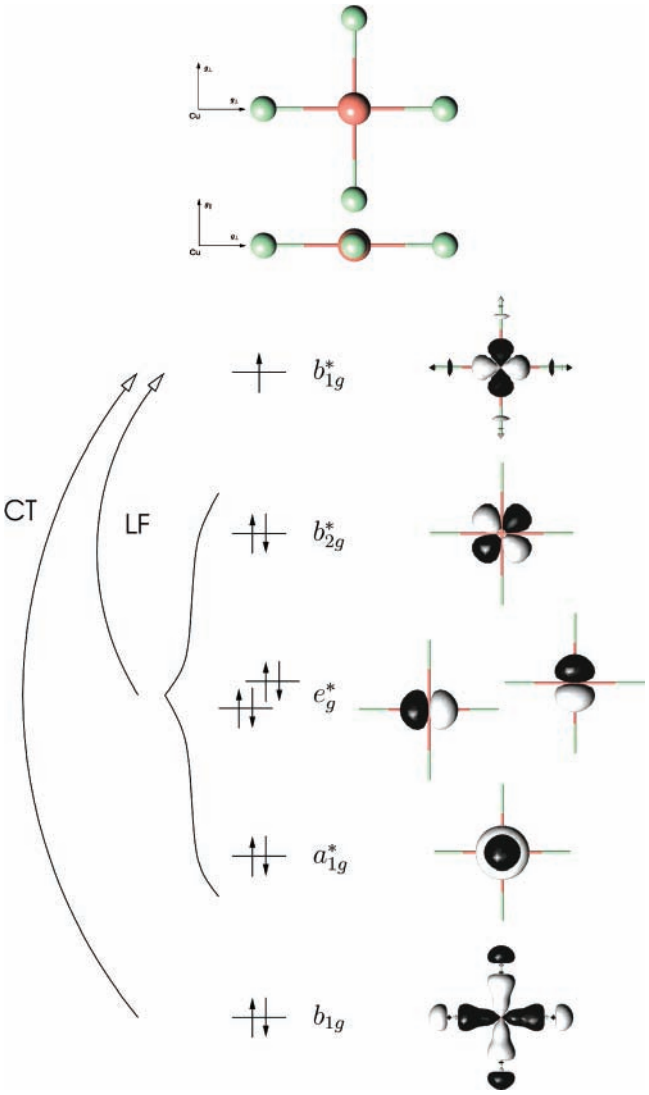

Figure 2. Schematic representation of the geometry and electronic structure of $[CuCl_4]^{2-}$.

The antibonding metal−ligand SOMO of the ground state in $[Cu(NH_3)_4]^{2+}$ and $[CuCl_4]^{2-}$ (b_2^* and b^*_{1g}, respectively) has its unpaired electron localized mainly on the copper center. The CT state where the corresponding bonding metal−ligand MO (b_2 and b_{1g}, respectively) is singly occupied has its unpaired electron localized mostly on the ligands. A state-averaged calculation including those states will significantly increase the covalency of both orbitals. As a result, the spin density on copper will drop together with the *g* values.

The results shown in the second column of Tables 1 and 2 were obtained from single-state CASPT2 calculations on each reference state. The use of state-averaged reference functions gives rise to a moderate increase of the excitation energies for both complexes, roughly 10% as compared to the state-specific results in the first column. On the other hand, the Δg values drop by approximately 16%. The relatively small change of the CASPT2 energies cannot fully account for the large change in *g* values. Hereto, a 20% increase in excitation energies would be required. The source of the remaining difference must be traced to smaller L and SO matrix elements, a result of the increased covalency (and thus smaller copper 3d contribution) of the SOMO in the ground-state CASSCF wave function. The latter effect is clear from the change in the copper 3d spin population, from 0.85 to 0.80 ($[Cu(NH_3)_4]^{2+}$) and 0.84 to 0.78 ($[CuCl_4]^{2-}$), a decrease of 5 and 7%, respectively. The Δg values

TABLE 1: Excitation Energies (cm^{-1}), Mulliken Spin Populations, and Δg Values (ppt) for $[Cu(NH_3)_4]^{2+}$

Excitation Energy				
	CASPT2			exp[43]
	SS[a]		MS[a]	
state	sep[b]	avg[b]		
a^2B_1	15163	16309	16679	14000
a^2E	16115	17283	17653	17500
a^2A_1	17243	18557	18926	16500
b^2B_2		51281	52021	
Δg Values				
	CASPT2			exp[44]
	SS[a]		MS[a]	
	sep[b]	avg[b]		
CASPT2 Approach I				
$\Delta g_{\parallel}$	81	67	59	45
$\Delta g_{\perp}$	360	301	264	239
CASPT2 Approach II				
$\Delta g_{\parallel}$	70	59	51	45
$\Delta g_{\perp}$	342	287	252	239
GS Mulliken Spin Population				
Cu	0.85	0.80	0.72	

[a] SS = single-state; MS = multistate. [b] sep = individually optimized orbitals; avg = using an average set of orbitals.

TABLE 2: Excitation Energies (cm^{-1}), Mulliken Spin Populations, and Δg Values (ppt) for $[CuCl_4]^{2-}$

Excitation Energy				
	CASPT2			exp[16]
	SS[a]		MS[a]	
state	sep[b]	avg[b]		
a^2B_{2g}	11321	12388	13465	12500
a^2E_g	13379	14445	15522	14200
a^2A_{1g}	14597	16170	17247	
b^2B_{1g}		37013	39167	
Δg Values				
	CASPT2			exp[45]
	SS[a]		MS[a]	
	sep[b]	avg[b]		
CASPT2 Approach I				
$\Delta g_{\parallel}$	96	81	58	47
$\Delta g_{\perp}$	466	387	277	230
CASPT2 Approach II				
$\Delta g_{\perp}$	78	67	48	47
$\Delta g_{\parallel}$	438	365	263	230
GS Mulliken Spin Population				
Cu	0.84	0.78	0.62	0.62[c]

[a] SS = single-state; MS = multistate. [b] sep = individually optimized orbitals; avg = using an average set of orbitals. [c] Experimental data from ref 42. Based on Xα scattered wave calculations with adjusted atomic sphere parameters to fit the experimental *g* values of $[CuCl4]^{2-}$.

obtained from the state-averaged calculation are considerably lower and closer to those from experiment than the results obtained from the state-specific GS calculation. However, we feel that this effect should be seen as artificial since the increased covalency was brought about by a worse description of the ground-state wave function at the CASSCF level of theory.

In order to improve the quality of the GS wave function, both states involved are in the next step allowed to mix under the influence of dynamical correlation by making use of the MS-

CASPT2 approach.[5] The results are shown in the third column of Tables 1 and 2. As a result of the second-order coupling between the $^2B_2$, $^2B_{1g}$ ground and charge-transfer state, the energy of the former state goes down, while the energy of the latter state rises. As there is no second-order coupling with other states, the absolute energies of the LF excited states do not change. The outcome is that the excitation energies of the LF states rise 2 and 7% for the ammine and chloride complex, respectively, as compared to the single-state results. The *g* values drop 13 ($[Cu(NH_3)_4]^{2+}$) and 28% ($[CuCl_4]^{2-}$). Clearly, the smaller L and SO matrix elements are the main source of the lowering of the *g* values. The ground-state Cu 3d spin population is lowered further by 10 and 20%, reflecting the increased covalency of the ground-state SOMO.

The multistate treatment thus shifts the ground-state wave function to a more covalent description by mixing the ground and excited charge-transfer states through dynamical correlation. Using the resulting new PMCAS (perturbation-modified CASSCF) reference functions significantly improves the *g* values. For $[Cu(NH_3)_4]^{2+}$, the ground-state Cu 3d spin population is 0.85 for the state-specific CASSCF wave function and 0.72 for the PMCAS wave function. In the case of the $[CuCl_4]^{2-}$ complex, the difference in the ground-state Cu 3d spin population between the state-specific CASSCF and PMCAS wave function is more pronounced, that is, 0.84 and 0.62, respectively. The latter value compares well with the ground-state experimental copper spin density of 0.62 ± 0.02 in $[CuCl_4]^{2-}$.[42] The difference in the Mulliken Cu 3d spin population between the two complexes has moved from 0.01 (column 1) to 0.10 (column 3), now clearly characterizing the Cu−Cl bond as more covalent than the Cu−NH_3 bond.

For both complexes, the final Δg values, obtained using the multistate approach, are generally in close agreement with experiment. All calculated values are still slightly too high, $\Delta g_{||}$ showing the largest deviations, 13−25 ppt for $[Cu(NH_3)_4]^{2+}$ and 33−47 ppt for $[CuCl_4]^{2-}$. These remaining errors are probably due to the neglect of environmental effects in the calculations since the experimental data were obtained either in solution for the ammine complex or in a crystalline environment for the chloride complex. Consistent with the changes in the spin populations, the effect of the multistate treatment on the *g* shifts is also largest for the chloride complex, that is, around −180 and −35 ppt for $\Delta g_{||}$ and $\Delta g_{\perp}$, respectively, as compared to only around −93 and −20 ppt for the ammine complex.

3.2. Plastocyanin. The active site in plastocyanin is composed of a central copper ion surrounded by four amino acid residues, bonded via two nitrogen atoms (His37, His87) and two sulfur atoms (Met92, Cys84), resembling a distorted tetrahedron. The unusually short copper−thiolate and long copper−thioether bonds from cysteine and methionine, respectively, are key characteristics of the (oxidized) blue copper active sites, related to their unique spectroscopic features. The latter include two absorption bands corresponding to charge-transfer excitations out of the bonding $Cu-S_{Cys}$ π and $Cu-S_{Cys}$ σ orbitals into the GS SOMO. The second CT transition is rather weak in plastocyanin but gains intensity in other blue copper proteins such as pseudoazurin and nitrite reductase. The intensity of these two bands is related to the large overlap between the S_{Cys} and Cu 3d orbitals, thus reflecting both a strongly covalent $Cu-S_{Cys}$ σ-type and π-type bond.

In order to understand the electronic spectrum of plastocyanin, a simple schematic picture of the active orbitals that are singly occupied in each of the states included in the calculations is presented in Figure 3. These are obtained by combining the five Cu 3d orbitals with two S_{Cys} 3p orbitals to form two $Cu-S_{Cys}$ bonding (π and σ) and two antibonding (π^* and σ^*) orbitals, together with three nonbonding Cu 3d orbitals (denoted as *n*). As 13 electrons are distributed over these 7 orbitals, the most antibonding orbital is singly occupied in the ground state. In plastocyanin, this is the antibonding $Cu-S_{Cys}$ π^* orbital. This is different from, for example, nitrite reductase where the SOMO gains considerably more $Cu-S_{Cys}$ σ^* character. The spectrum studied herein arises from excitations of a single electron out of each of the six doubly occupied orbitals into the singly occupied π^* orbital. Excitations out of the nonbonding Cu 3d and the antibonding σ^* orbital represent ligand field (LF) transitions, while those out of the bonding π and σ orbitals may be formally assigned as charge-transfer (CT) transitions. Figure 3 also shows the principal *g* axes, obtained by diagonalizing the symmetric part of the **g** tensor (for the PCU-S(PROT) model, basis B). The g_3 axis nearly coincides with the $Cu-S_{Met}$ bond (making an angle of 12.4°), while the g_2 and g_1 axes are situated (almost) in and perpendicular to the $S_{Cys}-Cu-S_{Met}$ plane, respectively.

The results (excitation energies, *g* shifts, and Cu/S_{Cys} spin populations,) obtained from MS-CASPT2 calculations on the different models described in section 2 are presented in Table 3. A first general observation is that the values of g_1 and g_2 are clearly dependent on the chosen approach, being smaller for approach II than for approach I. For the values of g_3, the difference is much less pronounced.

The results shown in the first four columns of Table 3 were obtained for the small PCU-S model. Going from column one to three, the protein surrounding is first neglected (VAC), then approximated by a medium with a dielectric constant of 4.0 (CONT), and finally taken into account by placing point charges around the model system (PROT). As the description of the surrounding is improved, all LF excitation energies decrease. The effect is smallest, about 700 cm^{-1}, for the $\sigma^* \rightarrow \pi^*$ transition, while for the three higher-lying LF transitions, it becomes as large as 2000−2500 cm^{-1}. Also for the CT states, the introduction of a dielectric medium has a quite strong stabilizing effect around 2000 cm^{-1}. However, it seems that in this case, the effect of the surrounding is overestimated by the dielectric medium model. If the protein is instead modeled as a collection of point charges, the CT energies are again increased. As a result, a net lowering of around 1000 cm^{-1} for the $\pi \rightarrow \pi^*$ transition and a status quo for the $\sigma \rightarrow \pi^*$ transition is observed, as compared to the vacuum results.

Together with the general energy decrease of the excited states, the GS spin populations are also clearly influenced by the protein surrounding. A steady increase of the spin population on Cu is observed as the description of the surrounding protein is improved, from 0.34 (VAC) to 0.41 (CONT) and further to 0.46 (PROT). It should be noted that, as opposed to that for the $[CuCl_4]^{2-}$ and $[Cu(NH_3)_4]^{2+}$ complexes, the unpaired electron in the GS of plastocyanin is not primarily localized on the copper atom but rather on the cysteine sulfur ligand. Also important to note is that these spin populations were obtained from the PMCAS ground-state wave function, that is, including dynamical correlation effects. At the CASSCF level, a much more ionic $Cu-S_{Cys}$ bond is found, with a spin population on Cu exceeding 0.80 (see further and Table 4).

The effect of the surrounding protein on the calculated *g* shifts is striking. For the vacuum PCU-S, all three calculated Δg values are too low as compared to experiment. For g_1 and g_2, the differences are small, 10−25 ppt. However, Δg_3 is underesti-

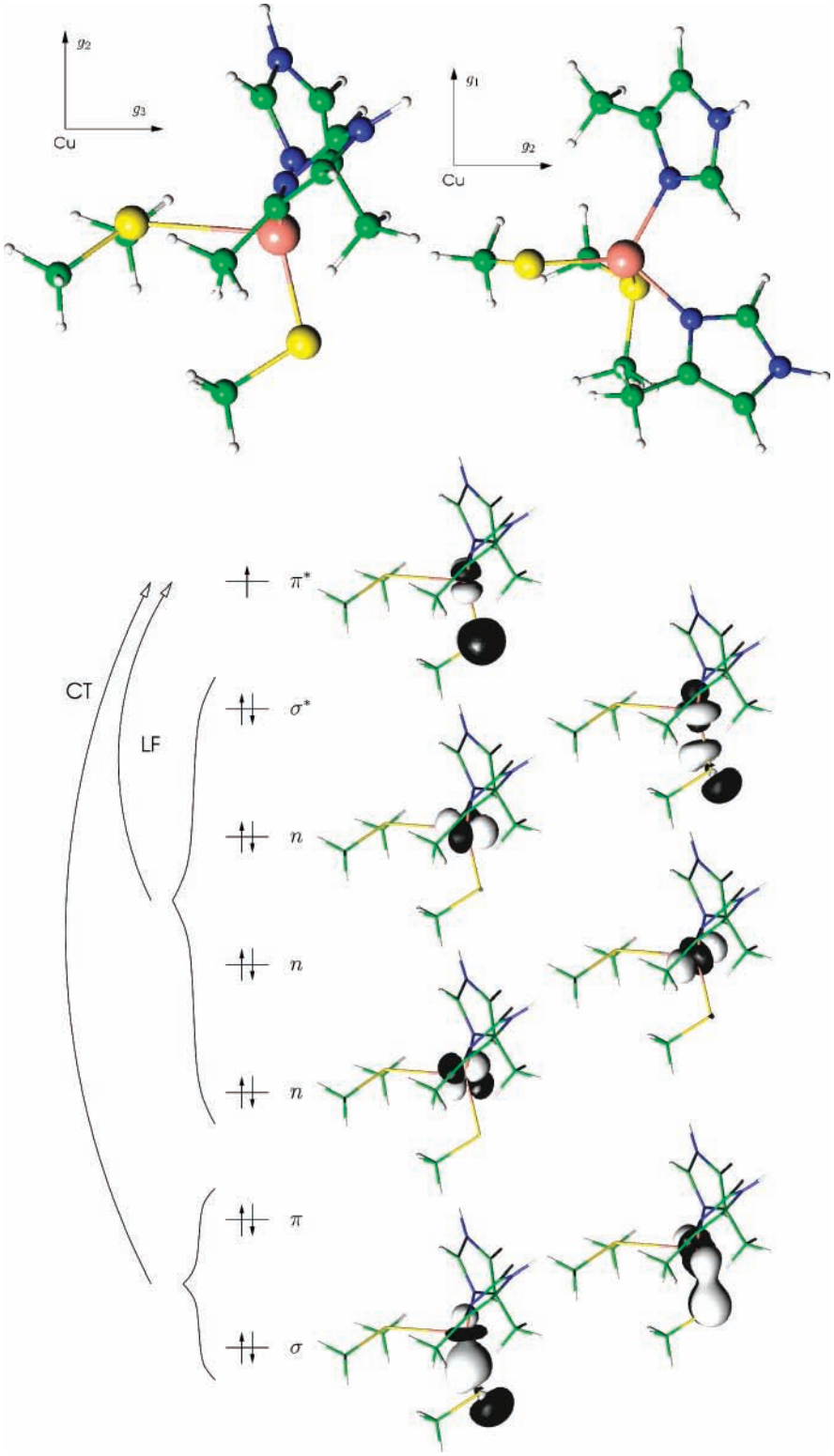

Figure 3. Schematic representation of the geometry and electronic structure of the PCU-S plastocyanin model.

mated by as much as 100 ppt. Including the protein environment increases all three g values, bringing them close to the experimental data. The effect is again largest for Δg_3 and is clearly better treated by means of point charges, giving a g_3 shift of almost 120 ppt, than with a continuum model, predicting only about half of this shift.

Column 5 shows the results obtained for the PCU-L model surrounded by point charges (PROT). For the calculations on this larger model, a smaller basis set (A) was used. For comparison, the smaller basis set was also used on the small PCU-S model (PROT), and these results are presented in column 4. As one can see, basis effects on the calculated excitation energies are limited (<200 cm^{-1}). However, the Δg values are significantly affected. In particular, the basis set reduction causes an increase of 20 ppt for Δg_3. This somewhat unexpectedly large difference should be brought back to (i) the larger flexibility of the contracted ANO-RCC basis on Cu in basis B ([5d2f1g] in B, [4d2f] in A), (ii) the larger flexibility of the primitive ANO-RCC (B) as compared to ANO-S (A) basis sets on the ligands, and (iii) the fact that relativistic effects are incorporated in the

TABLE 3: Excitation Energies (cm^{-1}), Mulliken Spin Populations, and Δg Values (ppt) for Different Plastocyanin Models

MS-CASPT2 Excitation Energies

basis	PCU-S (VAC) B	PCU-S (CONT) B	PCU-S (PROT) B	PCU-S (PROT) A	PCU-L (PROT) A	exp[7]
state						
LF($\sigma^* \rightarrow \pi^*$)	5912	5310	5197	5180	5331	5000
LF(n $\rightarrow \pi^*$)	16118	14313	13951	13762	13893	10800
LF(n $\rightarrow \pi^*$)	16956	15084	14536	14365	14472	12800
LF(n $\rightarrow \pi^*$)	18106	16339	15579	15374	15445	13950
CT($\pi \rightarrow \pi^*$)	19574	17300	18300	18283	18246	16700
CT($\sigma \rightarrow \pi^*$)	23764	21662	23691	23730	23733	21390

GS Mulliken Spin Populations

basis	PCU-S (VAC) B	PCU-S (CONT) B	PCU-S (PROT) B	PCU-S (PROT) A	PCU-L (PROT) A	exp[10,a]
			PMCAS			
Cu	0.34	0.41	0.46	0.48	0.47	0.41
S	0.63	0.56	0.51	0.50	0.50	
			DFT[24] (ZORA)			
Cu	0.35	0.39	0.44	0.44	0.43	0.41
S	0.54	0.50	0.43	0.43	0.43	

Δg Values

basis	PCU-S (VAC) B	PCU-S (CONT) B	PCU-S (PROT) B	PCU-S (PROT) A	PCU-L (PROT) A	exp[10]
			MS-CASPT2 Approach I			
Δg_1	30	39	50	53	51	45
Δg_2	45	51	59	61	59	57
Δg_3	127	186	246	266	255	224
			MS-CASPT2 Approach II			
Δg_1	22	26	31	32	32	45
Δg_2	36	37	38	38	38	57
Δg_3	122	179	235	253	243	224
			DFT[24] (ZORA)			
Δg_1	41	46	53	53	49	45
Δg_2	65	66	68	68	68	57
Δg_3	130	145	164	164	155	224

[a] Based on Xα scattered wave calculations with adjusted atomic sphere parameters to fit the experimental g values of $[CuCl_4]^{2-}$.

TABLE 4: Comparison of the CASPT2 and MS-CASPT2 Results for the PCU-S(PROT) Model (Results Obtained with Basis B)

root		CASPT2 results ΔE (cm^{-1})	CASPT2 spin popul Cu	CASPT2 spin popul S_{Cys}	CASPT2 contrib to Δg_3	MS-CASPT2 results ΔE (cm^{-1})	MS-CASPT2 spin popul Cu	MS-CASPT2 spin popul S_{Cys}	MS-CASPT2 contrib to Δg_3
1	GS		0.81	0.17			0.46	0.51	
2	LF($\sigma^* \rightarrow \pi^*$)	4063	0.82	0.17	727	5197	0.61	0.37	116
3	LF(n $\rightarrow \pi^*$)	11640	0.99	0.00	48	13950	0.95	0.04	24
4	LF(n $\rightarrow \pi^*$)	12529	0.98	0.01	15	14536	0.92	0.07	14
5	LF(n $\rightarrow \pi^*$)	13172	0.99	0.00	9	15579	0.99	0.01	0
6	CT($\pi \rightarrow \pi^*$)	12272	0.21	0.76	2	18300	0.66	0.33	2
7	CT($\sigma \rightarrow \pi^*$)	19905	0.33	0.64	78	23691	0.54	0.44	90
					879[a]				246[a]

[a] Totals of respective columns.

construction of the ANO-RCC basis sets, which is not the case for ANO-S. Comparing the results for the PCU-S(PROT) and PCU-L(PROT), we find that the effect of the extension of the central cluster model is limited, both for the excitation energies (with a maximum difference of 150 cm^{-1} for the LF $\sigma^* \rightarrow \pi^*$ state) and the spin populations. The largest effect is observed for the value of Δg_3, which is smaller by 8−10 ppt for PCU-L than that for PCU-S.

As compared to the experimental Δg values, the best results are obtained with the basis B calculations on the smaller PCU-S(PROT) model. With approach I, all Δg values are slightly too large, by 2−5 ppt for Δg_1 and Δg_2 and by 22 ppt for Δg_3. On the other hand, with approach II, the deviations for Δg_1 and Δg_2 are slightly larger and negative, −14 to −19 ppt, while the result for Δg_3 is improved, with a remaining error of only 11 ppt. Taking, somewhat tentatively, into account the 8−10 ppt reduction of Δg_3 upon increasing of the cluster model size (with the smaller basis A) would further reduce the remaining deviation of Δg_3 to less than 15 ppt with both approaches. On the whole, we may conclude that both sum-over-states-based

PMCAS/MS-CASPT2 approaches presented here are capable of predicting the g factors for this extended system with an accuracy that is close to quantitative.

In Table 3, we have also included the results for the spin populations and Δg values obtained for the same models by Sinnecker and Neese[24] with B3LYP-DFT, including scalar relativistic effects by means of the ZORA (zeroth-order regular approximation). Looking first at the vacuum PCU-S model, quite similar results are obtained with DFT and with the present MS-CASPT2 approach. The Cu spin density differs by only 0.01, and also for Δg_3, the results are close, 130 ppt from DFT and 122−127 ppt from MS-CASPT2. For Δg_1 and Δg_2, the differences are slightly larger, DFT predicting values that are larger by up to 30 ppt. However, although the introduction of the protein environment in the DFT calculations slightly reduces the Cu spin density more, the corresponding increase of g_3, 34 ppt, is much less pronounced than the increase of around 115 ppt computed with MS-CASPT2. As the authors of ref 24 note themselves, the underestimation of surrounding effects by DFT should be brought back to the fact that the linear response of the B3LYP functional (and other presently available functionals) is generally "too stiff" with respect to external perturbations. The effect of the size of the chosen model system on the computed g_3 shift with DFT, −9ppt, is again the same as that with MS-CASPT2.

It should be stressed that replacing the CASSCF/CASPT2 treatment with PMCAS/MS-CASPT2 is crucial for obtaining a correct description of the ground-state spin density and g shifts of the plastocyanin models. This is clearly illustrated by Table 4, comparing the results obtained from a CASPT2 and MS-CASPT2 treatment (both starting from the same set of average orbitals) for the PCU-S(PROT) model. In the previous section, it was shown for $[Cu(NH_3)_4]^{2+}$ and $[CuCl_4]^{2-}$ that by going from CASPT2 to MS-CASPT2, the results obtained for Δg are significantly improved, the major factor being a decrease of the copper 3d spin population resulting from the PMCAS wave function, giving rise to smaller L and SO matrix elements in the expression of the **g** tensor. Part of the reduction of the spin density was already obtained at the CASPT2 level by making use of the average instead of individually optimized CASSCF orbitals. In the case of plastocyanin, obtaining a different set of orbitals for each excited state is prevented by root flipping problems (giving rise to oscillating CASSCF iterations). Therefore, only CASPT2 results obtained with the same average set of orbitals for all states are shown in Table 4. A first glimpse at this table immediately points to the immense difference in the spin population on copper between the CASSCF and PMCAS wave functions, 0.81 versus 0.46. When performing an individual optimization for the ground state, an even higher number, 0.87, is obtained. Clearly, the problem with CASSCF giving a too ionic description of Cu−L bonds is more serious for the extremely covalent $Cu-S_{Cys}$ bond in plastocyanin than that for the Cu−Cl and $Cu-NH_3$ bonds in $[CuCl_4]^{2-}$ and $[Cu(NH_3)_4]^{2+}$.

For each excited state, Table 4 includes the excitation energy, the spin populations on Cu and S_{Cys}, and the contribution to the principal Δg_3 component. The states that are most strongly interacting in the MS-CASPT2 treatment are, on the one hand, the GS (root 1) and the CT($\pi \rightarrow \pi^*$) state (root 6), that is, states having the unpaired electron located in either the antibonding and bonding combination of Cu 3d and S_{Cys} $3p_\pi$, and, on the other hand, the first excited LF($\sigma^* \rightarrow \pi^*$) state (root 2) and the CT($\sigma \rightarrow \pi^*$) state (root 7), with the unpaired electron in either the antibonding and bonding combination of Cu 3d and S_{Cys} $3p_\sigma$. These interactions give rise to a stabilization of the GS and, to a lesser extent, the first excited state and to a concomitant destabilization of the corresponding CT states. As a result, the excitation energies of both CT states are quite strongly increased at the MS-CASPT2 as compared to the CASPT2 level, 6000 cm^{-1} for the CT($\pi \rightarrow \pi^*$) state and 3800 cm^{-1} for the CT($\sigma \rightarrow \pi^*$) state. The wave functions and absolute energies of the three more "pure" LF states (roots 3−5) are much less affected by the MS-CASPT2 treatment. Due to the GS stabilization, the excitation energies of these three states are increased by 2000−2400 cm^{-1}. It should be noted that the MS-CASPT2 treatment does not necessarily lead to an improved description of the excitation energies in the plastocyanin spectrum. Only the first LF state and, in particular, the first CT state are shifted closer to the corresponding experimental excitation energies (Table 3), while the upward shift of the other four states leads to errors of 1500−3000 cm^{-1}, as compared to a CASPT2 error of 800 cm^{-1} or less for the LF states and 1500 cm^{-1} for the second CT state.

However, a more important consequence of the MS-CASPT2 treatment is the strong redistribution of electron spin density between Cu and S_{Cys} in the PMCAS as compared to that in the CASSCF wave function. As one can see, CASSCF predicts an almost pure (>80%) Cu 3d SOMO both for the ground and the first excited LF state, while giving the SOMO of the two CT states predominant S_{Cys} character. In the PMCAS wave function, a thorough remixing of these four orbitals has occurred, such that all four SOMOs become an almost equal mixture of Cu 3d and S_{Cys} 3p. The main contributions to Δg_3 come from the two excited states with either the σ^* (root 2: LF) or σ (root 7: CT) singly occupied. At the CASSCF level, the L and SO matrix elements between the GS and the first LF state are grossly overestimated, giving rise to a Δg_3 contribution as large as 727 ppt! This situation is remedied in PMCAS by the strongly reduced Cu 3d character of both SOMOs, reducing this contribution to 116 ppt. The latter goes together with a slightly increased contribution to Δg_3 from the CT state, as the singly occupied σ orbital of this state now gains Cu 3d character. As one can see, two LF states also provide a small contribution to Δg_3, which is reduced in the PMCAS/MS-CASPT2 as compared to that with the CASSCF/CASPT2 treatment. However, the two main contributions, 116 and 90 ppt, come from excited states with either the bonding or antibonding σ combination of Cu 3d and S_{Cys} 3p depopulated. The importance of a well-described ground-state spin density distribution for obtaining accurate values for the g shifts in blue copper proteins has already been stressed in several previous studies.[6,10,12,16,23,25] Here, we have shown that an accurate description of the spin density distribution of these two excited states is equally important.

4. Conclusion

For all three Cu(II) complexes considered in this work, CASSCF gives a too ionic description of the copper−ligand bonds by providing the GS SOMO with too much Cu 3d character. This leads to considerable errors in the theoretical prediction of the EPR **g** tensors when employing CASSCF wave functions for the calculation of angular momentum and spin−orbit coupling matrix elements. For $[Cu(NH_3)_4]^{2+}$ and $[CuCl_4]^{2-}$, the problem was already detected in a previous paper,[1] where two different sum-over-states-based approaches for obtaining g values were proposed, both making use of a CASSCF/CASPT2 treatment of the ground and relevant excited states.

In this work, we propose to replace the CASSCF/CASPT2 treatment by a PMCAS/MS-CASPT2 treatment, including the

ground state with its predominant Cu 3d antibonding SOMO and the excited CT state where the corresponding, predominant ligand-based, bonding orbital is depopulated. By allowing these two states to mix under the influence of dynamical correlation, the description of the ground-state spin density distribution is considerably improved. Going from (GS-optimized) CASSCF to PMCAS, the spin population on Cu is decreased from 0.85 to 0.72 in $[Cu(NH_3)_4]^{2+}$, from 0.84 to 0.62 in $[CuCl_4]^{2-}$, and from 0.87 to 0.46 in plastocyanin. The latter numbers much more clearly reflect the expected increase in covalency of the Cu−L bonds within this series. For $[CuCl_4]^{2-}$ and plastocyanin, the PMCAS numbers also compare well to the experimental data, 0.62 and 0.41, respectively.

Both for $[Cu(NH_3)_4]^{2+}$ and $[CuCl_4]^{2-}$, the improved Δg values are close to experiment, with a maximum deviation of around 30 ppt. The same is true for plastocyanin, provided that the effect of the surrounding protein is properly taken into account. In order to describe this effect to its full extent, a set of (QM/MM-optimized) point charges rather than a dielectric medium is unavoidable. The present results for plastocyanin are clearly superior to a previous DFT study, making use of the same models[24] but underestimating the response of the electronic system to the external perturbation presented by the protein surrounding.

Altogether, we hope that the present results have convincingly demonstrated the strength of sum-over-states-based methods for obtaining EPR g values for large transition-metal systems, provided that they are combined with accurate ab initio wave functions/excitation energies.

Acknowledgment. This investigation was supported by the Flemish Science Foundation (FWO) and the Concerted Research Action of the Flemish Government (GOA). The authors thank F. Neese for providing the QM/MM structures of the plastocyanin models.

References and Notes

(1) Vancoillie, S.; Malmqvist, P.-Å.; Pierloot, K. *ChemPhysChem* **2007**, *8*, 1803−1815.

(2) Pierloot, K. Nondynamic Correlation Effects in Transition Metal Coordination Compounds. In *Computational Organometallic Chemistry*; Cundari, T. R., Ed.; Marcel Dekker: New York, 2000.

(3) Pierloot, K. *Mol. Phys.* **2003**, *101*, 2083−2094.

(4) Pierloot, K. Calculation of Electronic Spectra of Transition Metal Complexes. In *Computational Photochemistry, 16*; Olivucci, M., Ed.; Elsevier: Amsterdam, The Netherlands, 2005.

(5) Finley, J.; Malmqvist, P.-Å.; Roos, B. O.; Serrano-Andrés, L. *Chem. Phys. Lett.* **1998**, *288*, 299−306.

(6) Penfield, K. W.; Gewirth, A. A.; Solomon, E. I. *J. Am. Chem. Soc.* **1985**, *107*, 4519−4519.

(7) Gewirth, A. A.; Solomon, E. I. *J. Am. Chem. Soc.* **1988**, *110*, 3811−3819.

(8) Larsson, S.; Broo, A.; Sjölin, L. *J. Phys. Chem.* **1995**, *99*, 4860−4865.

(9) Pierloot, K.; De Kerpel, J. O. A.; Ryde, U.; Roos, B. O. *J. Am. Chem. Soc.* **1997**, *119*, 218−226.

(10) Solomon, E. I.; Szilagyi, R. K.; DeBeer George, S.; Basumallick, L. *Chem. Rev.* **2004**, *104*, 419−458.

(11) Pierloot, K.; De Kerpel, J. O. A.; Ryde, U.; Olsson, M. H. M.; Roos, B. O. *J. Am. Chem. Soc.* **1998**, *120*, 13156−13166.

(12) LaCroix, L. B.; Shadle, S. E.; Wang, Y.; Averill, B. A.; Hedman, B.; Hodgson, K. O.; Solomon, E. I. *J. Am. Chem. Soc.* **1996**, *118*, 7755−7768.

(13) LaCroix, L. B.; Randall, D. W.; Nersissian, A. M.; Hoitink, C. W. G.; Canters, G. W.; Valentine, J. S.; Solomon, E. I. *J. Am. Chem. Soc.* **1998**, *120*, 9621−9831.

(14) De Kerpel, J. O. A.; Pierloot, K.; Ryde, U.; Roos, B. O. *J. Phys. Chem. B* **1998**, *102*, 4638−4647.

(15) Palmer, A. E.; Randall, D. W.; Xu, F.; Solomon, E. I. *J. Am. Chem. Soc.* **1999**, *121*, 7138−7149.

(16) Neese, F.; Solomon, E. I. Interpretation and Calculation of Spin-Hamiltonian Parameters in Transition Metal Complexes. In *Magnetism: Molecules to Materials IV*; Miller, J. S., Drillon, M., Eds.; Wiley VCH: Weinheim, Germany, 2002.

(17) Ralle, M.; Berry, S. M.; Nilges, M. J.; Gieselman, M. D.; van der Donk, W. A.; Lu, Y.; Blackburn, N. J. *J. Am. Chem. Soc.* **2004**, *126*, 7244−7256.

(18) van Gastel, M.; Canters, G. W.; Krupka, H.; Messerschmidt, A.; de Waal, E. C.; Warmerdam, G. C. M.; Groenen, E. J. J. *J. Am. Chem. Soc.* **2000**, *122*, 2322−2328.

(19) Coremans, J. W. A.; Poluektov, O. G.; Groenen, E. J. J.; Warmerdam, G. C. M.; Canters, G. W.; Nar, H.; Messerschmidt, A. *J. Phys. Chem.* **1996**, *100*, 19706−19713.

(20) Solomon, E. I.; Hare, J. W.; Dooley, D. M.; Dawson, J. H.; Stephens, P. J.; Gray, H. B. *J. Am. Chem. Soc.* **1980**, *102*, 168−178.

(21) Solomon, E. I.; Penfield, K. W.; Gewirth, A. A.; Lowery, M. D.; Shadle, S. E.; Guckert, J. A.; Lacroix, L. B. *Inorg. Chim. Acta* **1996**, *243*, 67−78.

(22) Penfield, K. W.; Gewirth, A. A.; Solomon, E. I. *J. Am. Chem. Soc.* **1985**, *107*, 4519−4529.

(23) van Gastel, M.; Coremans, J. W. A.; Sommerdijk, H.; van Hemert, M. C.; Groenen, E. J. J. *J. Am. Chem. Soc.* **2002**, *124*, 2035−2041.

(24) Sinnecker, S.; Neese, F. *J. Comput. Chem.* **2006**, *27*, 1463−1475.

(25) Remenyi, C.; Reviakine, R.; Kaupp, M. *J. Phys. Chem. B* **2007**, *111*, 8290−8304.

(26) Malmqvist, P.-Å.; Rendell, A.; Roos, B. O. *J. Phys. Chem.* **1990**, *94*, 5477−5482.

(27) Andersson, K.; Malmqvist, P.-Å.; Roos, B. O.; Sadlej, A. J.; Wolinski, K. *J. Phys. Chem.* **1990**, *94*, 5483−5488.

(28) Andersson, K.; Malmqvist, P.-Å.; Roos, B. O. *J. Chem. Phys.* **1992**, *96*, 1218−1226.

(29) Karlström, G.; Lindh, R.; Malmqvist, P.-Å.; Roos, B. O.; Ryde, U.; Veryazov, V.; Widmark, P.-O.; Cossi, M.; Schimmelpfennig, B.; Neogrady, P.; Seijo, L. *Comput. Mater. Sci.* **2003**, *28*, 222−239.

(30) Douglas, M.; Kroll, N. M. *Ann. Phys.* **1974**, *82*, 89−115.

(31) Hess, B. A. *Phys. Rev. A* **1986**, *33*, 3742−3748.

(32) Wolf, A.; Reiher, M.; Hess, B. A. *J. Chem. Phys.* **2002**, *117*, 9215−9226.

(33) Forsberg, N.; Malmqvist, P.-Å. *Chem. Phys. Lett.* **1997**, *274*, 196−204.

(34) Ghigo, G.; Roos, B. O.; Malmqvist, P.-Å. *Chem. Phys. Lett.* **2004**, *396*, 142−149.

(35) Hess, B. A.; Marian, C. M.; Wahlgren, U.; Gropen, O. *Chem. Phys. Lett.* **1996**, *251*, 365−371.

(36) Christiansen, O.; Gauss, J.; Schimmelpfennig, B. *Phys. Chem. Chem. Phys.* **2000**, *2*, 965−971.

(37) Vahtras, O.; Engström, M.; Schimmelpfennig, B. *Chem. Phys. Lett.* **2002**, *351*, 424−430.

(38) Musiani, F.; Carloni, P.; Ciurli, S. *J. Phys. Chem. B* **2004**, *108*, 7495−7499.

(39) Siegbahn, P. E. M.; Blomberg, M. R. A.; Pavlov, M. *Chem. Phys. Lett.* **1998**, *292*, 421−430.

(40) Andersson, K.; Roos, B. O. *Chem. Phys. Lett.* **1992**, *191*, 507−514.

(41) Roos, B. O.; Andersson, K.; Fülscher, M. P.; Malmqvist, P.-Å.; Serrano-Andrés, L.; Pierloot, K.; Merchán, M. Multiconfigurational Perturbation Theory: Applications in Electronic Spectroscopy. In *Advances in Chemical Physics: New Methods in Computational Quantum Mechanics, Vol. XCIII:219*; Prigogine, I., Rice, S. A., Eds.; John Wiley & Sons: New York, 1996.

(42) Szilagyi, R. K.; Metz, M.; Solomon, E. I. *J. Phys. Chem. A* **2002**, *106*, 2994−3007.

(43) Neese, F. *Magn. Reson. Chem.* **2004**, *42*, S187−S198.

(44) Scholl, H.-J.; Hütterman, J. *J. Phys. Chem.* **1992**, *96*, 9684−9691.

(45) Chow, C.; Chang, K.; Willett, R. D. *J. Chem. Phys.* **1973**, *59*, 2629−2640.